Derivation of the phase-field-crystal model for colloidal solidification

Sven van Teeffelen,[1,*] Rainer Backofen,[2,†] Axel Voigt,[2] and Hartmut Löwen[1]
[1]*Institut für Theoretische Physik II, Weiche Materie, Heinrich-Heine-Universität Düsseldorf, D-40225 Düsseldorf, Germany*
[2]*Institute of Scientific Computing, Technical University Dresden, D-01062 Dresden, Germany*
(Received 19 February 2009; published 27 May 2009)

The phase-field-crystal model is by now widely used in order to predict crystal nucleation and growth. For colloidal solidification with completely overdamped individual particle motion, we show that the phase-field-crystal dynamics can be derived from the microscopic Smoluchowski equation via dynamical density-functional theory. The different underlying approximations are discussed. In particular, a variant of the phase-field-crystal model is proposed which involves less approximations than the standard phase-field-crystal model. We finally test the validity of these phase-field-crystal models against dynamical density-functional theory. In particular, the velocities of a linear crystal front from the undercooled melt are compared as a function of the undercooling for a two-dimensional colloidal suspension of parallel dipoles. Good agreement is only obtained by a drastic scaling of the free energies in the phase-field-crystal model in order to match the bulk freezing transition point.

DOI: 10.1103/PhysRevE.79.051404 PACS number(s): 82.70.Dd, 64.70.D−, 81.10.Aj

I. INTRODUCTION

Crystal-growth processes are relevant for a variety of different problems ranging from crystallization of proteins [1] and other biological macromolecules [2] over the construction of photonic crystals with an optical band gap [3] to applications in, e.g., metallurgy [4]. A full microscopic understanding of crystal growth with the interparticle interactions and the thermodynamic boundary conditions as the only input is still a great challenge since it requires a microscopic theory of freezing. Significant progress has been made by using the so-called *phase-field-crystal* (PFC) method in which the traditional phase-field theory [5] is generalized to a situation with a crystal order parameter. The PFC model was first developed by Elder and co-workers [6] and then subsequently applied to many other situations such as interfaces [7], polycrystalline pattern formation [8,9], crystal nucleation [10], commensurate-incommensurate transitions [11], and edge dislocations [12].

On the other hand, classical density-functional theory (DFT), which provides a microscopic theory for freezing in equilibrium [13–19], was generalized to nonequilibrium situations for colloidal particles with Brownian dynamics. The so-called dynamical density-functional theory (DDFT) can be derived from the basic Smoluchowski equation [20] and was found to be in very good agreement with Brownian dynamics computer simulations for dynamics in inhomogeneous situations [20–22] including crystal growth [23,24]. The PFC modeling possesses a *static* part invoking a free-energy expression for order parameters that describe the equilibrium bulk crystallization transition and a *dynamical* part that describes the evolution of the order parameters by a generalized diffusion or continuity equation.

Recently, Elder and co-workers derived the static free-energy input to the PFC model from microscopic equilibrium density-functional theory using a truncated density expansion [25]. This was supplemented by a gradient expansion in the order parameter [26,27]. However, a microscopic justification and derivation of the dynamical part is still missing. In this paper, we close this gap for colloidal suspensions where the individual dynamics is overdamped Brownian motion. Here, the appropriate microscopic starting point is the Smoluchowski equation [28,29] from which by an adiabatic approximation the dynamical density-functional theory can be derived [20]. In this paper we show that the dynamical density-functional theory provides a firm theoretical basis to derive the phase-field-crystal model and to discuss the approximations involved. We end up with two versions of the phase-field crystal model, referred to as the PFC1 and PFC2 models, which can both be implemented numerically with the same effort. We argue that the PFC1 model involves less approximations than the standard PFC2 model, which is traditionally used in phase-field crystal calculations.

Finally we compare the dynamics of freezing for DDFT and PFC modeling. The systems considered here are two-dimensional dipoles with parallel dipole moments pointing out of their confining plane. This system is realized for superparamagnetic colloidal particles which are confined to a two-dimensional air-water interface at a pending water droplet and exposed to an external magnetic field [30,31]. This system is characterized by the pairwise interaction potential $u(r)=u_0/r^3$, where u_0 is a parameter with dimensions of energy $\times$ volume. For the specific realization of two-dimensional paramagnetic colloids of susceptibility χ exposed to a perpendicular magnetic field $\mathbf{B}$, we have $u_0=(\chi\mathbf{B})^2/2$ in Gaussian units. As for all power-law interactions, the thermodynamics and structure depend only on one dimensionless coupling parameter $\Gamma=u_0\rho^{3/2}/k_BT$, where ρ is the average one-particle density and k_BT is the thermal energy.

For our comparison between the DDFT and the two PFC models we consider crystal growth out of an undercooled melt into a two-dimensional triangular crystal. The growth velocities of a linear crystal front, which is cut out of a perfect hexagonal lattice, are calculated as a function of the

*teeffelen@thphy.uni-duesseldorf.de
†rainer.backofen@tu-dresden.de

undercooling for both the PFC model and the DDFT. After renormalization of the excess part of the free energy, good agreement is obtained between both approaches implying that the PFC approach—with appropriately chosen input parameters—provides a reasonable and justified description framework of crystal-growth phenomena.

The outline of the paper is as follows. In Sec. II, we derive the DDFT from the Smoluchowski equation of overdamped Brownian motion in the same fashion as presented by Archer and Evans [20]. The approximate free-energy functional by Ramakrishnan and Yussouff (RY) [32] is incorporated into the DDFT in Sec. III. Subsequently, in Sec. IV, the two versions of the PFC model (PFC1 and PFC2) are derived from the approximate form of the DDFT. The different theories (DDFT, PFC1, and PFC2 models) are applied to crystal growth of dipoles in two dimensions (2D) in Sec. VI, including the presentation of the system's equilibrium phase diagram (Sec. VI A) and of the nonequilibrium problem (the setup description in Sec. VI B, and the results in Sec. VI C). In Sec. VII, we summarize and conclude.

II. DDFT

We consider the overdamped dynamics of a set of N identical, spherical, colloidal particles, immersed in a solvent, which serves for damping and as a heat bath. Assuming that the particles do not interact via hydrodynamic forces, the N-coupled Langevin equations of motion [28] are given by

$$\dot{\mathbf{r}}_i = \gamma^{-1}(\mathbf{F}_i + \mathbf{f}_i), \quad i = 1, \ldots, N, \tag{1}$$

where the dot denotes a time derivative and $\gamma = 3\pi\eta_0\sigma$ is the friction coefficient for a colloidal sphere with diameter σ in a fluid of viscosity η_0. For particles in an external field $V(\mathbf{r}_i, t)$, which interact with each other via pairwise additive potentials $u(|\mathbf{r}_i - \mathbf{r}_j|)$, the deterministic force acting on particle i is given by

$$\mathbf{F}_i(\{\mathbf{r}\}, t) = -\boldsymbol{\nabla}_i \left[\frac{1}{2} \sum_{i,j,i\neq j} u(|\mathbf{r}_i - \mathbf{r}_j|) + V(\mathbf{r}_i, t) \right], \tag{2}$$

where we denote the positions of all particles by $\{\mathbf{r}\} = \{\mathbf{r}_1, \ldots, \mathbf{r}_N\}$. The Gaussian white-noise random forces $\mathbf{f}_i$ originating from the solvent are characterized by the first two moments of their distribution function,

$$\langle \mathbf{f}_i(t) \rangle = \mathbf{0}, \tag{3}$$

$$\langle f_{i\alpha}(t) f_{j\beta}(t') \rangle = 2\gamma k_B T \delta_{ij} \delta_{\alpha\beta} \delta(t - t'), \tag{4}$$

where $k_B T$ is the thermal energy. The angle brackets denote a noise average and Greek indices indicate a component of the Cartesian vector. Equations (3) and (4) fulfill the well-known Einstein fluctuation-dissipation relation yielding a short-time diffusion constant $D = k_B T/\gamma$. The set of coupled, stochastic differential equations (1) for the particle coordinates corresponds to a deterministic Fokker-Planck equation for the N-particle probability density $W(\{\mathbf{r}\}, t)$ [28,29],

$$\dot{W}(\{\mathbf{r}\}, t) = \mathcal{L}_S W(\{\mathbf{r}\}, t), \tag{5}$$

$$\mathcal{L}_S = \gamma^{-1} \sum_i \boldsymbol{\nabla}_i [k_B T \boldsymbol{\nabla}_i - \mathbf{F}_i(\{\mathbf{r}\}, t)], \tag{6}$$

which determines the probability to find the set of N particles within a small volume around the positions $\{\mathbf{r}\}$ at time t, given a normalized, initial distribution $W(\{\mathbf{r}\}, t=0)$. The sum runs over all particles $i = 1, \ldots, N$. The continuity Eq. (5) is referred to as Smoluchowski equation [28].

For dense, strongly interacting fluids, one is typically not interested in the position of all individual particles but rather in the probability to find *any* particle at a certain vector $\mathbf{r}$ at time t. We therefore introduce the time-dependent one- and two-particle densities

$$\rho(\mathbf{r}, t) = \sum_i \langle \delta[\mathbf{r} - \mathbf{r}_i(t)] \rangle, \tag{7}$$

$$\rho^{(2)}(\mathbf{r}, \mathbf{r}', t) = \sum_{i,j;i\neq j} \langle \delta[\mathbf{r} - \mathbf{r}_i(t)] \delta[\mathbf{r} - \mathbf{r}_j(t)] \rangle, \tag{8}$$

where we dropped the superscript "(1)" on the one-particle density. Generally, the n-particle density is equal to the $(N-n)$-times integrated probability density W,

$$\rho^{(n)}(\mathbf{r}_1, \ldots, \mathbf{r}_n, t) = \frac{N!}{(N-n)!} \int d^{N-n}\mathbf{r} W(\{\mathbf{r}\}, t). \tag{9}$$

A deterministic equation of motion for the time evolution of $\rho(\mathbf{r}, t)$ [Eq. (10)] can on the one hand be directly derived from the Langevin equations, Eq. (1), via a coordinate transformation $\mathbf{r}_i \to \hat{\rho}(\mathbf{r}, t) = \Sigma_i \delta[\mathbf{r}(t) - \mathbf{r}_i(t)]$ is the one-particle density operator, and a subsequent noise average. This way was followed by Marconi and Tarazona (MT) [21], based on an earlier approach by Dean [33]. On the other hand, the same equation is obtained by integrating the Smoluchowski equation (5) over the positions of $N-1$ of the N particles and making use of Eqs. (7)–(9). The latter approach was adopted by Archer and Evans [20]. The continuity equation for $\rho(\mathbf{r}, t)$ reads

$$\dot{\rho}(\mathbf{r}, t) = \gamma^{-1} \boldsymbol{\nabla} [k_B T \boldsymbol{\nabla} \rho(\mathbf{r}, t) + \rho(\mathbf{r}, t) \boldsymbol{\nabla} V(\mathbf{r}, t) + \int d\mathbf{r}' \rho^{(2)}(\mathbf{r}, \mathbf{r}', t) \boldsymbol{\nabla} u(|\mathbf{r} - \mathbf{r}'|)]. \tag{10}$$

For noninteracting particles in zero external field, this equation reduces to Fick's diffusion equation. Also with an external field applied, Eq. (10) is exactly solvable. In the interesting case of interacting particles, however, an expression for the time-dependent two-particle density $\rho^{(2)}(\mathbf{r}, \mathbf{r}', t)$ is still needed.

Within DDFT, $\rho^{(2)}(\mathbf{r}, \mathbf{r}', t)$ is approximated by a yet unspecified equilibrium two-particle density $\rho_0^{(2)}(\mathbf{r}, \mathbf{r}')$; the latter is evaluated at a corresponding equilibrium fluid, in which the equilibrium density $\rho_0(\mathbf{r})$ is equal to the instantaneous one-particle density $\rho(\mathbf{r}, t)$ of the nonequilibrium system. The approximation of replacing a time-dependent, nonequilibrium by an equilibrium correlation function is referred to as *adiabatic* approximation; it goes back to Enskog [34], who applied it to the time evolution of the single-particle distribution function in a dense gas of hard spheres. In order to render the instantaneous density $\rho(\mathbf{r}, t)$ an equilibrium

density, an appropriate external potential $v(\mathbf{r})$ must be applied. That such a potential exists for any physical density field $\rho(\mathbf{r},t)$ and that it is, further, a unique functional of the density $\rho_0(\mathbf{r})$ is stated and proved in one of the basic theorems of density-functional theory [35].

The connection to classical density-functional theory is now made by identifying the three different terms in the bracket on the right-hand side of Eq. (10) with terms of the form $\rho(\mathbf{r})\nabla\delta F_i[\rho]/\delta\rho(\mathbf{r})$, where the $F_i[\rho]$ are different contributions to the Helmholtz free-energy functional $F[\rho(\mathbf{r})]$, which is provided by classical density-functional theory. The functional $F[\rho(\mathbf{r})]$ is a unique functional of the static one-particle density $\rho(\mathbf{r})$ [35]. If $F[\rho(\mathbf{r})]$ is known exactly it is minimized by the equilibrium one-particle density $\rho(\mathbf{r})=\rho_0(\mathbf{r})$, where it takes the value of the Helmholtz free energy $F\equiv F[\rho_0(\mathbf{r})]$. The functional is divided into three terms:

$$F[\rho(\mathbf{r})] = F_{\mathrm{id}}[\rho(\mathbf{r})] + F_{\mathrm{ex}}[\rho(\mathbf{r})] + F_{\mathrm{ext}}[\rho(\mathbf{r})]. \tag{11}$$

The ideal-gas part, which is of completely entropic nature and which yields the (first) diffusion term in Eq. (10), is

$$F_{\mathrm{id}}[\rho(\mathbf{r})] = k_BT\int d\mathbf{r}\rho(\mathbf{r})\{\ln[\rho(\mathbf{r})\Lambda^d]-1\}, \tag{12}$$

with Λ denoting the thermal de Broglie wavelength and d the spatial dimension. The external part corresponding to the second term in Eq. (10) is given by

$$F_{\mathrm{ext}}[\rho(\mathbf{r})] = \int d\mathbf{r}\rho(\mathbf{r})V(\mathbf{r},t). \tag{13}$$

Finally, the excess part $F_{\mathrm{ex}}[\rho(\mathbf{r})]$, originating from the correlations between the particles, is generally unknown and must be approximated; a specific approximation is introduced further down. Note that the excess part is *not* the potential energy of interaction but a contribution to the free energy. The connection of the excess part and the third term on the right-hand side of Eq. (10) is made through the sum rule

$$-\rho_0(\mathbf{r})\nabla c_0^{(1)}(\mathbf{r}) = (k_BT)^{-1}\int d\mathbf{r}'\rho_0^{(2)}(\mathbf{r},\mathbf{r}')\nabla u(|\mathbf{r}-\mathbf{r}'|), \tag{14}$$

which connects the two-particle density $\rho_0^{(2)}(\mathbf{r},\mathbf{r}')$ with the effective one-body potential $k_BTc_0^{(1)}(\mathbf{r})$. The latter, in turn, is—up to a minus sign—equal to the first functional derivative of the excess free-energy functional $F_{\mathrm{ex}}[\rho_0(\mathbf{r})]$ with respect to density,

$$k_BTc_0^{(1)}(\mathbf{r}) = -\frac{\delta F_{\mathrm{ex}}[\rho_0(\mathbf{r})]}{\delta\rho(\mathbf{r})}. \tag{15}$$

Using Eqs. (14) and (15), we can therefore rewrite Eq. (10) as

$$\dot{\rho}(\mathbf{r},t) = \gamma^{-1}\left\{k_BT\nabla^2\rho(\mathbf{r},t) + \nabla\cdot[\rho(\mathbf{r},t)\nabla V(\mathbf{r},t)] - \nabla\cdot\left[\rho(\mathbf{r},t)\nabla\frac{\delta F_{\mathrm{ex}}[\rho(\mathbf{r},t)]}{\delta\rho(\mathbf{r},t)}\right]\right\}, \tag{16}$$

which, making use of Eqs. (11)–(13), reads in a compact form

$$\dot{\rho}(\mathbf{r},t) = \gamma^{-1}\nabla\cdot\left[\rho(\mathbf{r},t)\nabla\frac{\delta F[\rho(\mathbf{r},t)]}{\delta\rho(\mathbf{r},t)}\right]. \tag{17}$$

Equation (17) constitutes the fundamental, nonlinear, deterministic equation for the time evolution of the one-particle density $\rho(\mathbf{r},t)$ and will be referred to as DDFT equation henceforth. For time-independent external potentials $V(\mathbf{r})$, the DDFT describes the relaxation dynamics of the density field toward equilibrium at the minimum of the Helmholtz free-energy functional $F[\rho_0]$, given an exact canonical excess free-energy functional $F_{\mathrm{ex}}[\rho]$. The path in the space of density fields is in general not the one of steepest descent, but is governed by the mass-conservation constraint in Eq. (17) [21].

Equation (17) is a deterministic equation; it has no extra noise term, as all the fluctuations—given that $F_{\mathrm{ex}}[\rho]$ is exact—are already taken into account. As discussed at large by MT [21,36], the addition of a noise term in Eq. (16) leads to an overcounting of fluctuations. Archer and Rauscher discussed the possibility of including a noise term if $\rho(\mathbf{r},t)$ is not interpreted as the ensemble averaged but as a coarse-grained (in time) probability distribution $\bar{\rho}(\mathbf{r},t)$ [37]. However, this also requires a replacement of the functional $F[\rho]$ by a functional of the coarse-grained probability density, which is *not* the Helmholtz free-energy functional of density-functional theory. We will come back to this point in Sec. V.

The DDFT equation was suggested earlier on phenomenological grounds by Evans [35] and later by Dieterich *et al.* [38]. The same dynamical equation with the excess free-energy functional of Ramakrishnan and Yussouff [32,39] (cf. Sec. III) was derived by Munakata [40,41] and extended to nonspherical particles in the context of solvation dynamics by Calef and Wolynes [42], which was later reformulated by Chandra and Bagchi [43,44]; these equations are referred to as Smoluchowski-Vlasov or *nonlinear diffusion* equations [41] as they are derived from a Vlasov equation [45] with a Fokker-Planck collision operator [41]. However, MT were the first to derive the theory from the microscopic equations of motion and to make clear the contact to static DFT [21,36]. Similar attempts were made by other authors before (Kirkpatrick [46], Dean [33], and Kawasaki and Miyazima [47,48]), which, however, do not distinguish the average density ρ with the density operator $\hat{\rho}$, which in turn leads to an additional noise term on the right-hand side of Eq. (17) and therefore to an overcounting of fluctuations, given an accurate functional $F[\rho]$ (see also the discussions by MT [21], Archer and Rauscher [37], and Löwen [49]).

The DDFT is an approximate theory in several respects: the first and most fundamental approximation is the already introduced assumption of adiabatic relaxation dynamics. In practice, this approximation is most severe in dynamical pro-

cesses that are fast compared to the diffusive time scale of the system. To our knowledge, this issue has been studied systematically to date only for weak perturbations of a hard-rod fluid in one dimension by Penna and Tarazona [50]. The use of approximate free-energy functionals is the second fundamental approximation turning out to be severe in many applications (cf. the next section). Third, we did only consider systems in which hydrodynamic interactions between the particles play no role. The latter assumption can be approximately tackled by allowing for density-dependent friction constants γ [51], which is appropriate for long-wavelength fluctuations of the density field or by taking hydrodynamic interactions on the Rotne-Prager (two-particle) level into account, as was recently demonstrated by Rex and Löwen [52].

III. APPROXIMATE DENSITY-FUNCTIONALS IN THE DDFT

For most problems including those involving freezing, $F_{\mathrm{ex}}[\rho(\mathbf{r})]$ is only known approximately [14,35]; in practice, this restriction most often constitutes the more severe approximation as compared to the adiabatic approximation. In this paper, we follow the approach of Ramakrishnan and Yussouff [32] as laid out for the dipolar system in 2D in Ref. [53] and as already exploited for the DDFT of the same model in Refs [23,24]. Within the RY approach, $F_{\mathrm{ex}}[\rho(\mathbf{r})]$ is expanded up to second order in terms of density difference $\Delta\rho=\rho(\mathbf{r})-\rho$ around a reference fluid, where the fluid density ρ is chosen the average density of the inhomogeneous system

$$F_{\mathrm{ex}}[\rho(\mathbf{r})] \simeq F_{\mathrm{ex}}(\rho) - \frac{k_B T}{2}\int\int d\mathbf{r}d\mathbf{r}'\Delta\rho(\mathbf{r})\Delta\rho(\mathbf{r}') \times c_0^{(2)}(\mathbf{r}-\mathbf{r}';\rho). \tag{18}$$

Here $F_{\mathrm{ex}}(\rho)$ and $c_0^{(2)}(\mathbf{r};\rho)$ are the excess free energy and the direct correlation function of the reference fluid of density ρ, respectively [54]. Despite the ease of implementation the RY excess free-energy functional is used here because it will lead directly to the PFC model in the next section. Within the RY approximation the DDFT equation now reads

$$\dot{\rho}(\mathbf{r},t) = D\{\nabla^2\rho(\mathbf{r},t) + (k_B T)^{-1}\boldsymbol{\nabla}\cdot[\rho(\mathbf{r},t)\boldsymbol{\nabla}V(\mathbf{r},t)] - \boldsymbol{\nabla}\cdot[\rho(\mathbf{r},t)\boldsymbol{\nabla}\int d\mathbf{r}'\rho(\mathbf{r}')c_0^{(2)}(|\mathbf{r}-\mathbf{r}'|;\rho)]\}, \tag{19}$$

with $D=k_B T/\gamma$ the diffusion constant.

Apart from leading to quantitatively wrong equilibrium density fields and free energies the approximate density functional might display more than one local minimum, in which the system might get trapped. For example, in conjunction with freezing a flat and constant density profile, corresponding to the fluid state, is "metastable" at all temperatures for any known approximate density functional; starting from the fluid state, within DDFT, the system therefore never reaches the stable crystalline state which is represented through a periodically modulated density field. As discussed at length by MT [21,36], this failure made some groups add a noise term to Eq. (17), which is at best justified *a posteriori*. In particular, it leads to the already-mentioned overcounting of fluctuations (see also Sec. V).

IV. PFC MODEL

As the DDFT, the PFC model is based on a free-energy functional $\mathcal{F}[\psi(\mathbf{r},t)]$ of a phase field $\psi(\mathbf{r},t)$ and a dynamical equation for the phase field's time evolution similar to the DDFT equation. The PFC model was introduced as a phenomenological theory by Elder *et al.* [6,55]. If the yet to be specified functional $\mathcal{F}[\psi(\mathbf{r},t)]$ is set equal to a particular approximation of the Helmholtz free-energy functional from density-functional theory, i.e., $\mathcal{F}[\psi(\mathbf{r},t)]=F[\rho(\mathbf{r},t)=\psi(\mathbf{r},t)]$, as was also suggested by Elder *et al.* [25], the phase field is consequently to be interpreted as the density field, i.e., $\psi(\mathbf{r},t)=\rho(\mathbf{r},t)$. We show in this section that the commonly used PFC equation of motion [6,55] [Eq. (27)] can be regarded as a particularly simplified and further-approximated version of the DDFT with the RY approximation to the excess free-energy functional [cf. Eq. (19)]; consequently, the PFC model is derived here from the basic Langevin equations of motion (1) for the case of overdamped dynamics. Of course, this reasoning only holds if the phase field $\psi(\mathbf{r},t)$ in the PFC model is regarded as the density field $\rho(\mathbf{r},t)$ of Eq. (7), which will be assumed in this section and is believed to be assumed in many other papers whenever $\mathcal{F}[\psi]$ is set equal to $F[\rho]$. Different interpretations of $\psi(\mathbf{r},t)$ are discussed in the next section.

Apart from the adiabatic and the RY approximation the derivation goes via three further approximations. First, the RY excess free-energy functional, Eq. (18), is approximated by a (local) gradient expansion. Second, the mobility in the dynamical equation (19) is set to be constant, i.e., $\gamma^{-1}\rho(\mathbf{r},t)\approx\gamma^{-1}\rho$, with ρ the *average* density of the system. Third, the ideal-gas part of the free energy, Eq. (12), is approximated by its truncated Taylor series. According to the (additional) approximations of the PFC model, two different equations of motion are put forward: referred to as the PFC1 model, which is obtained after the first approximation, and as the PFC2 model, which is obtained after the second and third approximations. Obviously, the PFC2 model constitutes an approximate form of the PFC1 model.

Following the procedure suggested by Elder and coworkers [25], the RY excess free-energy functional, Eq. (18), is approximated by its gradient expansion within both PFC approaches

$$\mathcal{F}_{\mathrm{ex}}[\rho(\mathbf{r})] = F_{\mathrm{ex}}(\rho) - \frac{k_B T}{2}\int d\mathbf{r}\Delta\rho(\mathbf{r}) \times(\hat{C}_0 - \hat{C}_2\nabla^2 + \hat{C}_4\boldsymbol{\nabla}^4 + \cdots)\Delta\rho(\mathbf{r}). \tag{20}$$

Consequently, $\mathcal{F}_{\mathrm{ex}}$ is *local* in the density field, which renders the yet to be introduced PFC equations of motion [approximate forms of the DDFT equation (19)] computationally faster to solve. The gradient expansion is equivalent to a Taylor expansion of the Fourier transform $\hat{c}_0^{(2)}(\mathbf{k};\rho)$ of the two-particle direct correlation function introduced in Eq. (18),

$$\hat{c}_0^{(2)}(\mathbf{k};\rho) = \hat{C}_0 + \hat{C}_2 k^2 + \hat{C}_4 k^4 + \cdots . \tag{21}$$

Due to rotational symmetry of the pair-correlation function the expansion is only in even powers of k. Truncating the expansion at fourth order, the time evolution given by Eq. (17) now reads

$$\dot{\rho}(\mathbf{r},t) = D\nabla^2\rho(\mathbf{r},t) + D\,\boldsymbol{\nabla}\cdot\{\rho(\mathbf{r},t)\,\boldsymbol{\nabla}\,[(k_BT)^{-1}V(\mathbf{r},t) - (\hat{C}_0 - \hat{C}_2\nabla^2 + \hat{C}_4\boldsymbol{\nabla}^4)\rho(\mathbf{r},t)]\}. \tag{22}$$

This equation, which we refer to as PFC1 model, approximates the integrodifferential equation of the DDFT, Eq. (17), by a local partial differential equation of sixth order. Further down, we will advocate the use of this equation rather than of the more approximate equation of the PFC2 model.

The (second) constant-mobility approximation, an *ad hoc* assumption of a constant density $\rho(\mathbf{r},t)=\rho$ in front of the functional derivative in Eq. (17), leads to the equation

$$\dot{\rho}(\mathbf{r},t) = \gamma^{-1}\rho\nabla^2\left[\frac{\delta\mathcal{F}[\rho(\mathbf{r},t)]}{\delta\rho(\mathbf{r},t)}\right], \tag{23}$$

where the total free-energy functional is given by

$$\mathcal{F}[\rho] = F_{\mathrm{id}}[\rho] + F_{\mathrm{ext}}[\rho] + \mathcal{F}_{\mathrm{ex}}[\rho]. \tag{24}$$

Concurrently, insertion of the ideal-gas part of the Helmholtz free-energy functional, Eq. (12), leads to a term, which is logarithmic in the density field,

$$\nabla^2\left[\frac{\delta F_{\mathrm{id}}[\rho(\mathbf{r},t)]}{\delta\rho(\mathbf{r},t)}\right] = k_BT\nabla^2\,\ln[\rho(\mathbf{r},t)\Lambda^d]. \tag{25}$$

This term replaces the simpler diffusion term, $\nabla^2\rho(\mathbf{r},t)$, in the DDFT equation (and in the PFC1 model). Within the PFC2 model the logarithm is expanded in a power series about the constant density ρ, i.e.,

$$F_{\mathrm{id}}[\rho(\mathbf{r})] \approx k_BT\rho\int d\mathbf{r}\left\{\frac{1}{2}\phi(\mathbf{r},t)^2 - \frac{1}{6}\phi(\mathbf{r},t)^3 + \frac{1}{12}\phi(\mathbf{r},t)^4 - \mathrm{const.}\right\}, \tag{26}$$

with $\phi(\mathbf{r},t)=[\rho(\mathbf{r},t)-\rho]/\rho$ the dimensionless density modulation. This leads to the standard form of the PFC model used in the literature,

$$\dot{\phi}(\mathbf{r},t) = D\rho\nabla^2\left[\phi(\mathbf{r},t) - \frac{1}{2}\phi(\mathbf{r},t)^2 + \frac{1}{3}\phi(\mathbf{r},t)^3 + (k_BT)^{-1}V(\mathbf{r},t) - \rho(\hat{C}_0 - \hat{C}_2\nabla^2 + \hat{C}_4\boldsymbol{\nabla}^4)\phi(\mathbf{r},t)\right], \tag{27}$$

which is henceforth referred to as the constitutive equation of the PFC2 model. Note that the second and third terms on the right-hand side only appear due to the constant-mobility assumption and are not present in the less-approximate Eq. (22).

We will use the (standard) PFC2 model, Eq. (27), as well as the more accurate PFC1 model, Eq. (22), and compare them to the DDFT, employing the RY approximation, Eq. (19). Therefore we need to parametrize $\hat{C}_0, \hat{C}_2$, and $\hat{C}_4$ in the PFC1 and PFC2 models according to $\hat{c}(\mathbf{k};\Gamma)$ in Eq. (21). A particular parametrization, motivated from the *one-mode* approximation to the PFC2 model [55], is chosen and presented in Sec. VI. Before we come to the comparison we comment shortly on the use of an additional noise term in Eqs. (22) and (27) in the following section.

V. NOISE TERM IN THE PFC EQUATION

Typically, the PFC2 equation (27) is supplemented by a nonmultiplicative Gaussian noise term $\eta(\mathbf{r},t)$ [6] fulfilling

$$\langle\eta(\mathbf{r},t)\rangle = 0, \tag{28}$$

$$\langle\eta(\mathbf{r},t)\,\eta(\mathbf{r}',t')\rangle = 2k_BT\gamma^{-1}\delta(\mathbf{r}-\mathbf{r}')\,\delta(t-t'). \tag{29}$$

As already pointed out in Sec. II, such a noise term cannot be derived in the context of DDFT since the density field $\rho(\mathbf{r},t)$ is an ensemble-averaged quantity. Instead, the addition of a noise term in Eq. (16) leads to an overcounting of fluctuations [21]. Therefore we point out that—at least for colloidal dynamics—the addition of a noise term is not well justified.

However, Archer and Rauscher [37] argue on a phenomenological basis that a noise term fulfilling Eqs. (28) and (29) can be introduced if the phase field is *not* understood as the ensemble-averaged probability density $\rho(\mathbf{r},t)$ but as a coarse-grained (in time) density

$$\bar{\rho}(\mathbf{r},t) = \int_{-\infty}^{t} dt'\,K(t-t')\hat{\rho}(\mathbf{r},t'), \tag{30}$$

with $K(t)$ a coarse-graining function of width $\tau=\int_0^\infty dttK(t)$ and $\hat{\rho}(\mathbf{r},t)=\Sigma_i\delta[\mathbf{r}(t)-\mathbf{r}_i(t)]$ the density operator, as already introduced above. However, if this approach is followed, the functional $F[\rho]$ needs to be replaced by a functional of the coarse-grained probability density $\bar{\rho}(\mathbf{r},t)$, which is *not* the Helmholtz free-energy functional of density-functional theory and which is generally unknown. Second, the temperature entering Eq. (29) must be renormalized by a factor $\sqrt{\tau_0/\tau}$ accounting for the ratio of the microscopic time scale τ_0 and the coarse-graining time scale τ. In fact, the dependence of Eq. (29) on τ_0 points to a conflict with a fundamental assumption of Brownian dynamics, namely, that τ_0 is much smaller than any relevant time scale. If this reasoning is followed nevertheless, the nonmultiplicative nature of the noise term, Eq. (28), comes about only after an approximation similar to the one of constant mobility in the PFC2 model whereas the less-approximate PFC1 model should be appended by a multiplicative noise term of the form

$$\eta(\mathbf{r},t) \to \boldsymbol{\nabla}\sqrt{\frac{\tau_0}{\tau}\bar{\rho}(\mathbf{r},t)}\,\eta(\mathbf{r},t), \tag{31}$$

where the gradient assures mass conservation. Due to the gradient the Îto and Stratonovich calculus [28] are equivalent. For a phenomenological motivation of the according dynamical equation, we refer the reader to Archer and Rauscher [37]. In the following, we do not consider a fluctuating density field but restrict our study to the application of the deterministic DDFT, PFC1, and PFC2 equations, respec-

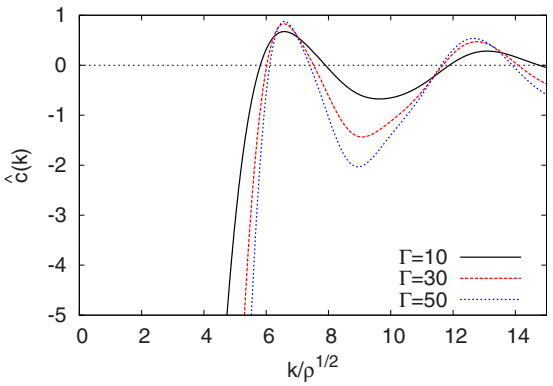

FIG. 1. (Color online) The Fourier transform $\hat{c}(k)$ of the two-particle direct correlation function for different coupling constants $\Gamma=10,30,50$ plotted against $k/\rho^{1/2}$.

tively. Finally, we remark that a noise term in the case of molecular dynamics was recently discussed by Tupper and Grant [56].

VI. APPLICATION OF THE DDFT AND THE PFC MODEL TO PROPAGATING CRYSTAL FRONTS

In this and the following section, we compare the three different approaches to the nonequilibrium Brownian dynamics discussed, the DDFT, and the two PFC models to the problem of propagating crystal fronts. For a better understanding of what drives the crystal growth, we present, first, the equilibrium phase diagram obtained from the underlying free-energy functionals in Sec. VI A before studying the dynamics in Sec. VI B.

A. Equilibrium state

Input to the static free-energy functionals, Eqs. (11) and (24), and, concurrently, to the dynamical theories is the direct correlation function of the fluid $c_0^{(2)}(\mathbf{r})$ [57], which has been obtained for a large range of coupling constants $0<\Gamma\leq 62.5$ from liquid-state integral equation theory as described in Refs. [53,58]. In particular, $c_0^{(2)}(\mathbf{r})$ has been obtained by iteratively solving the coupled Ornstein-Zernicke equation [57] and the closure relation suggested by Rogers and Young [59]. The dimensionless Fourier transform of the pair-correlation function $\hat{c}(k)=\rho\tilde{c}_0^{(2)}(k)$ as a function of wave vector is plotted for different coupling constants Γ in Fig. 1.

Whereas the excess free energy in the RY approximation to the DFT, Eq. (18), requires, in general, the complete correlation function $\hat{c}(k)$, the respective function in the PFC models, Eq. (20), only needs the parameters $\hat{C}_0,\hat{C}_2$, and $\hat{C}_4$ as an input. The latter can in principle be obtained from $\hat{c}(k)$ in different ways. For our purpose they are chosen according to a series expansion of $\hat{c}(k)$ in terms of k^2 about the correlation function's first maximum at $k=k^*$ up to second order in k^2, i.e.,

$$\hat{c}(k) \simeq \hat{C}_0+\hat{C}_2k^2+\hat{C}_4k^4 = \hat{c}(k^*)+(k^2-k^{*2})\hat{c}'(k^*)+\frac{1}{2}(k^2-k^{*2})^2\hat{c}''(k^*). \tag{32}$$

Here, primes denote derivatives with respect to k^2. Another way to determine the coefficients [25] is a fit which reproduces the isothermal compressibility at $k\to 0$, the bulk modulus, and the lattice constant of the crystal.

As a subsequent motivation of the suggested fit and also for an estimate of the phase behavior, we calculated the Helmholtz free energy of the PFC2 model analytically in the *one-mode* approximation [55]. Within this approximation, the two-dimensional density field is assumed to be sinusoidal and hexagonally symmetric, i.e.,

$$\phi(x,y)\approx A\left[\frac{1}{2}\cos(kx)-\cos\left(\frac{\sqrt{3}kx}{2}\right)\cos\left(\frac{ky}{2}\right)\right], \tag{33}$$

with an amplitude A and a nearest-neighbor distance of $a=2\pi/k$. Equation (33) together with Eqs. (20) and (26) yield the free energy per particle

$$\frac{\mathcal{F}(A,k)}{N}=\frac{A^2}{512}\{15A^2-16A+96[1-\hat{c}(k)]\}. \tag{34}$$

Minimization with respect to k and A gives the equilibrium wave number $k=k^*$ and the equilibrium amplitude

$$A^*(\rho)=\begin{cases}0, & \hat{c}(k^*;\rho)<c_f\\ \frac{2}{5}\{[20\hat{c}(k^*;\rho)-19]^{1/2}+1\}, & \hat{c}(k^*;\rho)>c_f,\end{cases} \tag{35}$$

where $c_f=43/45=0.956$. The first line corresponds to the stable fluid and the second to the stable crystal phase, respectively. For values of $c_u<\hat{c}(k^*;\rho)<c_f$, with $c_u=0.95$, the crystalline density field is metastable, i.e., the free energy, Eq. (34), has a local, nonglobal minimum at a finite amplitude A. For values $\hat{c}(k^*;\rho)<c_u$, the crystal is unstable toward collapse. As the approximate free energy, Eq. (34), in the PFC model is governed by $\hat{c}(k^*)$, a proper representation of the latter is on order and a series expansion of $\hat{c}(k)$ about k^* appears natural.

The RY approximation to the DFT predicts a stable crystal for $\Gamma>\Gamma_f^{\mathrm{DFT}}\approx 36.5$ and a metastable crystal for $\Gamma_u\lesssim\Gamma<\Gamma_f$, with $\Gamma_u\approx 31$ [53]. The coupling constant at freezing Γ_f corresponds to a maximum value of the correlation function of $\hat{c}(k^*;\Gamma_f)=:c_f^{\mathrm{DFT}}\approx 0.843$, which is substantially smaller than the value of $c_f=0.956$, obtained in the one-mode approximation. On the other hand, extrapolation of $\hat{c}(k^*;\Gamma)$ to a value of $c_f=0.956$ yields a freezing transition within the one-mode approximation to the PFC2 model of $\Gamma_f\approx 100$, as can be seen in Fig. 2. In order to obtain a similar stability regime of the crystalline solution to the DDFT and to the PFC2 and PFC1 models, the excess free energy of the PFC models is rescaled by a factor of $f=1.15$ independent of Γ. The phase behaviors of both PFC models without the constraint on the functional form of the density field of Eq. (33) are similar but slightly different than in the one-mode approximation; it is discussed in Sec. VI C.

B. Nonequilibrium dynamics: Setup description

In order to measure the propagation front velocities predicted by the DDFT, Eq. (17) is numerically solved on a

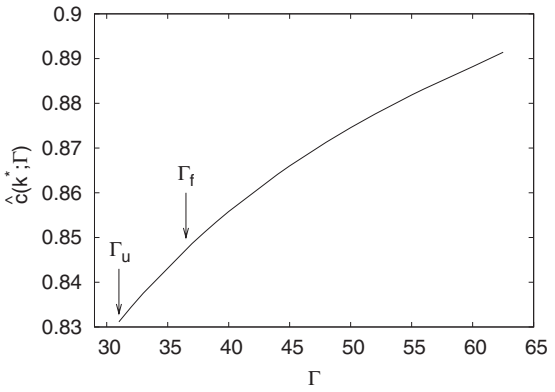

FIG. 2. The maximum of the correlation function $\hat{c}(k^*;\Gamma)$ vs the interaction strength Γ. The arrows at Γ_u and Γ_f bracket the range of metastability of the crystalline density field, obtained from the RY approximation to the DFT.

rectangular periodic box of a fine grid with ~64 grid points per nearest-neighbor distance a. A finite difference method with variable time step is applied. The convolution integrals are solved using the method of fast Fourier transform. The two versions of the PFC model, Eqs. (22) and (27), are solved by finite-element methods with a variable time step. The sixth-order partial differential equations are solved semi-implicitly as a system of second-order partial differential equations [10].

We study the propagation dynamics of the front of a linear array along the y direction, which is a cutout of a perfect hexagonal crystal and comprises, at $t=0$, a number of s infinite rows of particles centered about $x=0$, as can be exemplarily seen from the density map for $t=0$ in Fig. 3 for $\Gamma=60$. The number of crystalline rows s is chosen larger than the critical nucleus to guarantee crystal growth [24] for $\Gamma > \Gamma_f$ or reasonably large in order to study crystal shrinkage for $\Gamma < \Gamma_f$ [60]. The size of the periodic, rectangular box is therefore chosen integer multiples of the lattice spacing of the perfectly ordered hexagonal crystal,

FIG. 3. (Color online) Snapshots of the dimensionless, logarithmic density field $\log_{10}[\rho(\mathbf{r},t)/\rho]$ of a linear nucleus of initially $s=5$ (DDFT; top panel) or $s=11$ (PFC1 model; bottom panel) infinite rows of hexagonally crystalline particles at coupling constant $\Gamma=60$, as obtained from the DDFT (top panel) and the PFC1 model (bottom panel). The upper and the lower four maps show the density fields each at times $t/\tau_B=0,0.5,1,1.5$ (from top to bottom). For better visibility and exploiting the symmetry of the density field, the images display twice the right half of the system's central region of dimensions $35\sqrt{3}/2a \times 2a$.

$$L_x \times L_y = 128(\sqrt{3}/2)a \times a. \tag{36}$$

The nearest-neighbor distance is fixed to its ideal value

$$a = (2/\sqrt{3})^{1/2}\rho^{-1/2}, \tag{37}$$

which is very close to the equilibrium value of the one-mode approximation to the PFC2 model, $a=2\pi/k^*$, and to the equilibrium value of the RY approximation to the DFT for all values of Γ [53]. The initial density field is given by

$$\rho(\mathbf{r},t=0) = [1-h(|x|-R)]\rho_c(\mathbf{r}) + h(|x|-R)\rho. \tag{38}$$

Here, $h(x)$ is a smoothed approximation to the Heaviside step function. $\rho_c(\mathbf{r})$ is the infinite, stable or metastable, crystalline density field with constrained lattice constant a and with the [11]-orientation parallel to the x axis, which is symmetric about $x=0$. The size of the initial nucleus is defined by $R=(\sqrt{3}/4)sa$, with s the number of crystalline rows parallel to the y axis. $h(|x|-R)$ is therefore chosen to cut through valleys of the density field guaranteeing the overall particle number to be fixed, i.e., $V^{-1}\int_V d\mathbf{r}\rho(\mathbf{r},t=0)=\rho$. For the number of crystalline rows for the different coupling constants, see [60].

The initial density field $\rho(\mathbf{r},t=0)$ can be thought of as an equilibrium density field with an appropriately chosen, though somewhat artificial, external potential $V(\mathbf{r})$ [13]. An experimentally more feasible and thus more realistic setup has been suggested in Ref. [24]. The array of tagged particles was first, i.e., for times $t<0$, held fixed in a thermodynamically stable, equilibrated fluid of density ρ at a coupling constant $\Gamma < \Gamma_f$ well-below freezing. For the equilibration of the fluid, Eq. (17) was numerically solved fixing the tagged particles by deep parabolic external potentials at the tagged particle positions—in an experiment this could be achieved by using optical tweezers [61]. At time $t=0$ the external pinning potential was turned off and, at the same time, the system was instantaneously quenched to a higher coupling constant Γ. Experimentally, the instantaneous quench is easily achieved by increasing the homogeneous external magnetic field $\mathbf{B}$. Both protocols lead to different short-time dynamics $[t \lesssim (\rho D)^{-1}]$ due to the initial difference in the density field close to the incipient cluster. However, for longer times the density fields are indistinguishable (data not shown) thus leading to the same propagation front velocities which are of interest in this work.

C. Nonequilibrium dynamics: Results

In Fig. 3, we display the density field $\rho(\mathbf{r},t)$ as obtained from the DDFT and from the rescaled PFC2 model for $\Gamma=60$ at four different times $t/\tau_B=0,0.5,1,1.5$, where we chose the Brownian time scale $\tau_B=(\rho D)^{-1}$ as the unit time scale. Since the density field is symmetric with respect to the x axis we concentrate on the region $x>0$ in the following. Figure 4 displays the corresponding y-averaged density profile,

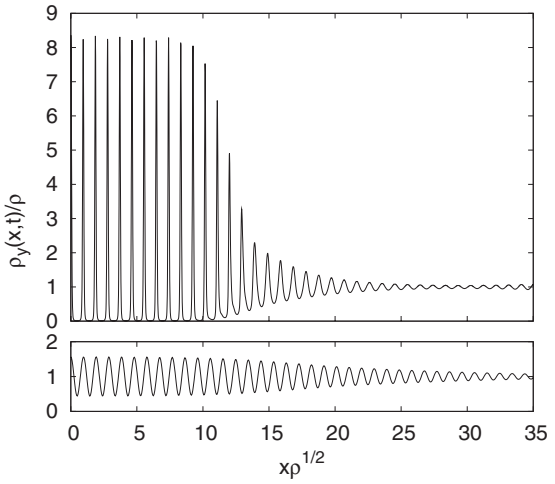

FIG. 4. The y-average density profile $\rho_y(x,t=\tau_B)$ obtained from the DDFT (top panel) and the PFC1 model (bottom panel) for the same coupling constant $\Gamma=60$ and the same initial conditions as in Fig. 3 at the time $t/\tau_B=1$.

$$\rho_y(x,t) \equiv L_y^{-1} \int dy \rho(\mathbf{r},t), \tag{39}$$

at a short time $t=\tau_B$, which is large enough for $\rho_y(\mathbf{r},t)$ to be insensitive on the details of the same field at time $t=0$. Density fields obtained within the rescaled PFC1 model are qualitatively very similar to the ones of the PFC2 model; they are therefore not displayed in the present paper.

It can be ascertained from Fig. 3 that after short time the propagating crystal fronts approximately establish steady states, which eventually change on larger time scales $t \gg \tau_B$ [62]. As can also be seen from Figs. 3 and 4, the crystalline density fields behind the crystal fronts, which are close to equilibrium in all three models, are modulated much stronger about the average density ρ in the DDFT than in the two rescaled PFC models. This difference goes along with an almost sinusoidal density field in the PFC models, approximately equal to the field assumed in the one-mode approximation, Eq. (33), which is due to the truncation of the expansion of $F_{\text{ex}}[\rho]$ in k^2 [Eq. (20)]; this density field is in contrast to the one of the DDFT, which is approximately given by a superposition of Gaussians centered about the lattice vectors of the hexagonal lattice. Another qualitative difference between the two models concerns the crystal-melt interface: the width of the crystal front obtained within the DDFT is substantially smaller than in the PFC models; whereas the former is of the order of $\Delta x \sim 5\rho^{-1/2}$, the latter approximately amounts $\Delta x \sim 25\rho^{-1/2}$. In both models, the widths are relatively insensitive toward changes in coupling constant Γ (data not shown).

In order to quantify the crystal front propagation, the position of the diffuse front, $x_f(t)$, is extracted as the maximum x position at which the density field exceeds the value 2ρ, in the DDFT, and as the inflection point of the envelope function to $\rho_y(x,t)$ in the PFC model, respectively (data not shown). Within the DDFT, the front position is thus situated at a position, which is at the same time slightly larger than

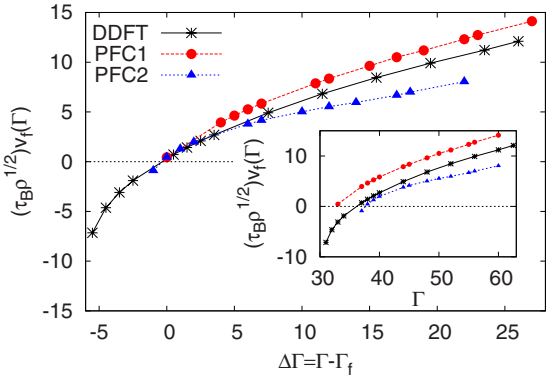

FIG. 5. (Color online) Propagation front velocities of a linear crystal front in the [11]-direction, $v_f(\Gamma)$, measured shortly after the quench (see text), as a function of relative coupling constant $\Delta\Gamma=\Gamma-\Gamma_f$, with Γ_f the respective coupling constant of freezing, obtained within the DDFT (stars), the PFC1 model (circles), and the PFC2 model (triangles). Lines are guides to the eyes. Inset: the same velocities as a function of Γ.

the one in the PFC models. However, this does not affect the crystal front velocity $v_f(\Gamma)=\partial x_f(t)/\partial t$, which was measured as a function of coupling constant Γ for the three different models under study at a short distance from the incipient front, $x_f(t=0)+15\rho^{-1/2} < x_f(t) < x_f(t=0)+20\rho^{-1/2}$ (see Fig. 5). The front velocity at long times is not considered in this paper [62]. Comparing the three different curves of Fig. 5, the following observations are made:

(i) In all three models, $v_f(\Gamma)$ increases monotonically from 0 with increasing difference in coupling constant $\Delta\Gamma \equiv \Gamma-\Gamma_f$, where the freezing constant is $\Gamma_f=36.5$ within the DFT [23], $\Gamma_f \approx 33$ in the rescaled PFC1 model, and $\Gamma_f \approx 38$ within the rescaled PFC2 model. The three coupling constants do not agree because the rescaling of the excess free energy was chosen to bring only the freezing constants of the more approximate one-mode approximation to the PFC2 model into agreement with the freezing constant of the DFT. The same scaling is then used for the PFC1 and PFC2 models without the constraint of a sinusoidal density field, Eq. (33). The difference between the respective values within the PFC1 and the PFC2 models is due to the difference in their respective ideal free energies $F_{\text{id}}[\rho]$, Eqs. (12) and (26). Moreover, as the ideal free-energy functionals of the DFT and the PFC1 model are equal, the freezing constant of the rescaled PFC1 model is lower than the one of the rescaled PFC2 model, which is reminiscent of the smaller distance of the respective freezing constants within the nonrescaled models (obtained from an extrapolation of $\hat{c}(k)$; data not shown).

(ii) For negative $\Delta\Gamma$, with Γ still within the metastability regime, $\Gamma_u < \Gamma < \Gamma_f$, the propagation front velocity is negative, and a retraction of an almost steady-state crystal front is observed.

(iii) For $\Delta\Gamma > 0$, the front velocities obtained within the two rescaled PFC models bracket the respective values obtained within the DDFT, the PFC1 model being slightly closer to the DDFT as the PFC2 model. All three models yield similar front velocities, although the corresponding steady-state density fields are quite different (see Fig. 4).

However, the nonmonotonicity of the propagation front velocities $v_f(\Delta\Gamma)$ for the same value of $\Delta\Gamma$ with increasing degree of approximation (from the DDFT via the PFC1 model to the PFC2 model) points to a cancellation of errors in the approximate PFC models. Still, as would have been expected, the velocities obtained from the less-approximate PFC1 model are closer to the results of the DDFT than those of the more approximate PFC2 model.

VII. CONCLUSIONS

In conclusion, we have derived the PFC model from microscopic DDFT appropriate for colloidal dispersions, which are governed by completely overdamped Brownian dynamics. The ordinary phase-field-crystal model (called PFC2 model) arises from a constant-mobility approximation *and* an expansion of the ideal-gas entropy in terms of density. Both approximations can be avoided yielding a variant of the phase-field-crystal model (called PFC1 model), which requires the same computational effort as the PFC2 model.

Comparing the two phase-field-crystal models to the full solution of the dynamical density-functional theory, agreement could only be obtained by an empirical scaling factor in the free energy. On the one hand, this implies that phase-field-crystal models have to be used with care and lack full *ab initio* precision. If a suitable scaling is accepted, there is good overall agreement in the growth velocity of a crystalline front, where the PFC1 model yields slightly better agreement than the PFC2 model. The corresponding density fields, however, differ vastly in terms of the sharpness of the crystalline peaks. We therefore conclude that the phase-field-crystal model gives a qualitative reliable description of the trends in crystal-growth processes but lacks high precision.

Future work should focus, first, on three-dimensional crystalline fronts and on the dynamics and annealing of crystalline defects, where both DDFT and PFC models should be compared as well. Second, the behavior of the setup at intermediate and long times deserves more detailed study. Finally, full Brownian dynamics computer simulations [24] are needed to obtain reference data for a test of the underlying adiabatic approximation in the DDFT.

ACKNOWLEDGMENTS

We thank R. Blaak and C. N. Likos for helpful discussions. This work has been supported by the DFG through the DFG Priority Program No. SPP 1296.

[1] M. C. Wiener, Methods **34**, 364 (2004).
[2] E. H. Snell and J. R. Helliwell, Rep. Prog. Phys. **68**, 799 (2005).
[3] N. V. Dziomkina and G. J. Vancso, Soft Matter **1**, 265 (2005).
[4] H. Emmerich, K. Binder, and B. Nestler, Philos. Mag. Lett. **87**, 791 (2007).
[5] H. Emmerich, Adv. Phys. **57**, 1 (2008).
[6] K. R. Elder, M. Katakowski, M. Haataja, and M. Grant, Phys. Rev. Lett. **88**, 245701 (2002).
[7] B. P. Athreya, N. Goldenfeld, J. A. Dantzig, M. Greenwood, and N. Provatas, Phys. Rev. E **76**, 056706 (2007).
[8] K. A. Wu and A. Karma, Phys. Rev. B **76**, 184107 (2007).
[9] N. Goldenfeld, B. P. Athreya, and J. A. Dantzig, Phys. Rev. E **72**, 020601(R) (2005).
[10] R. Backofen, A. Ratz, and A. Voigt, Philos. Mag. Lett. **87**, 813 (2007).
[11] C. V. Achim, M. Karttunen, K. R. Elder, E. Granato, T. Ala-Nissila, and S. C. Ying, Phys. Rev. E **74**, 021104 (2006).
[12] J. Berry, M. Grant, and K. R. Elder, Phys. Rev. E **73**, 031609 (2006).
[13] D. W. Oxtoby, *Liquids, Freezing and the Glass Transition*, Les Houches Summer Schools of Theoretical Physics, LI, 1989 (North Holland, Amsterdam, 1991), p. 147.
[14] Y. Singh, Phys. Rep. **207**, 351 (1991).
[15] H. Löwen, Phys. Rep. **237**, 249 (1994).
[16] H. Löwen, J. Phys.: Condens. Matter **14**, 11897 (2002).
[17] C. N. Likos, Phys. Rep. **348**, 267 (2001).
[18] M. Rex, H. Löwen, and C. N. Likos, Phys. Rev. E **72**, 021404 (2005).
[19] M. Rex, C. N. Likos, H. Löwen, and J. Dzubiella, Mol. Phys. **104**, 527 (2006).
[20] A. J. Archer and R. Evans, J. Chem. Phys. **121**, 4246 (2004).
[21] U. M. B. Marconi and P. Tarazona, J. Chem. Phys. **110**, 8032 (1999).
[22] J. Dzubiella and C. N. Likos, J. Phys.: Condens. Matter **15**, L147 (2003).
[23] H. Löwen, C. N. Likos, L. Assoud, R. Blaak, and S. van Teeffelen, Philos. Mag. Lett. **87**, 847 (2007).
[24] S. van Teeffelen, C. N. Likos, and H. Löwen, Phys. Rev. Lett. **100**, 108302 (2008).
[25] K. R. Elder, N. Provatas, J. Berry, P. Stefanovic, and M. Grant, Phys. Rev. B **75**, 064107 (2007).
[26] H. Löwen, T. Beier, and H. Wagner, Europhys. Lett. **9**, 791 (1989); Z. Phys. B: Condens. Matter **79**, 109 (1990).
[27] J. F. Lutsko, Physica A **366**, 229 (2006).
[28] H. Risken, *The Fokker-Planck Equation, Methods of Solution and Applications*, 2nd ed. (Springer-Verlag, Berlin, 1989).
[29] M. von Smoluchowski, Ann. Phys. **353**, 1103 (1916).
[30] K. Zahn, J. M. Méndez-Alcaraz, and G. Maret, Phys. Rev. Lett. **79**, 175 (1997).
[31] R. Haghgooie and P. S. Doyle, Phys. Rev. E **72**, 011405 (2005).
[32] T. V. Ramakrishnan and M. Yussouff, Phys. Rev. B **19**, 2775 (1979).
[33] D. S. Dean, J. Phys. A **29**, L613 (1996).
[34] D. Enskog, K. Sven. Vetenskapsakad. Handl. **63**, 4 (1922) [English translation in *Kinetic Theory*, edited by S. G. Brush (Pergamon Press, London, 1972), Vol. 3, p. 226].
[35] R. Evans, Adv. Phys. **28**, 143 (1979).
[36] U. M. B. Marconi and P. Tarazona, J. Phys.: Condens. Matter **12**, A413 (2000).
[37] A. Archer and M. Rauscher, J. Phys, A **37**, 9325 (2004).

[38] W. Dieterich, H. L. Frisch, and A. Majhofer, Z. Phys. B: Condens. Matter **78**, 317 (1990).
[39] A. D. J. Haymet and D. W. Oxtoby, J. Chem. Phys. **74**, 2559 (1981).
[40] T. Munakata, J. Phys. Soc. Jpn. **43**, 1762 (1977).
[41] T. Munakata, J. Phys. Soc. Jpn. **43**, 1723 (1977).
[42] D. F. Calef and P. G. Wolynes, J. Chem. Phys. **78**, 4145 (1983).
[43] A. Chandra and B. Bagchi, J. Chem. Phys. **91**, 1829 (1989).
[44] A. Chandra and B. Bagchi, Physica A **169**, 246 (1990).
[45] P. Résibois and M. DeLeener, *Classical Kinetic Theory of Fluids* (John Wiley, New York, 1977).
[46] T. R. Kirkpatrick, J. Phys. A **22**, L149 (1989).
[47] K. Kawasaki and S. Miyazima, Z. Phys. B: Condens. Matter **103**, 423 (1997).
[48] K. Kawasaki, Physica A **208**, 35 (1994).
[49] H. Löwen, J. Phys.: Condens. Matter **15**, V1 (2003).
[50] F. Penna and P. Tarazona, J. Chem. Phys. **124**, 164903 (2006).
[51] C. P. Royall, J. Dzubiella, M. Schmidt, and A. van Blaaderen, Phys. Rev. Lett. **98**, 188304 (2007).
[52] M. Rex and H. Löwen, Phys. Rev. Lett. **101**, 148302 (2008).
[53] S. van Teeffelen, H. Löwen, and C. N. Likos, J. Phys.: Condens. Matter **20**, 404217 (2008).
[54] Note that the static properties of the dipolar system under study, including the equilibrium phase diagram, have been obtained applying different and more accurate approximations to the excess free-energy functional [53,58].
[55] K. R. Elder and M. Grant, Phys. Rev. E **70**, 051605 (2004).
[56] P. F. Tupper and M. Grant, Europhys. Lett. **81**, 40007 (2008).
[57] J.-P. Hansen and I. R. McDonald, *Theory of Simple Liquids*, 3rd ed. (Academic Press, London, 2006).
[58] S. van Teeffelen, C. N. Likos, N. Hoffmann, and H. Löwen, Europhys. Lett. **75**, 583 (2006).
[59] F. J. Rogers and D. A. Young, Phys. Rev. A **30**, 999 (1984).
[60] In particular, we chose $s=60$ for $31 \leq \Gamma \leq 35$, $s=7$ for $37 \leq \Gamma < 40$, and $s=5$ for $\Gamma \geq 40$, in the DDFT, $s=41$ for $\Gamma=33$, $s=21$ for $\Gamma=37$, $s=11$ for $38 \leq \Gamma \leq 60$, in the PFC1 model, and $s=83$ for $\Gamma=37$, $s=41$ for $\Gamma=38$, $s=21$ for $\Gamma=39$, and $s=11$ for $38 \leq \Gamma \leq 60$ in the PFC2 model.
[61] M. Köppl, P. Henseler, A. Erbe, P. Nielaba, and P. Leiderer, Phys. Rev. Lett. **97**, 208302 (2006).
[62] The discussion of the behavior of $v_f(t \gg \tau_B)$ in the DDFT and the PFC models is deferred to a future publication. For the same behavior in a similar model of hard spheres, see [63].
[63] R. Wild and P. Harrowell, J. Chem. Phys. **114**, 9059 (2001).